Bumetanide induces post-traumatic microglia-interneuron contact to promote neurogenesis and recovery

Marine Tessier, Marta Saez Garcia, Emmanuelle Goubert, Edith Blasco, Amandine Consumi, Benoit Dehapiot, Li Tian, Florence Molinari, Jerome Laurin, François Guillemot, et al.

Bumetanide induces post-traumatic microglia–interneuron contact to promote neurogenesis and recovery

Marine Tessier,[1] Marta Saez Garcia,[2] Emmanuelle Goubert,[1] Edith Blasco,[1] Amandine Consumi,[1] Benoit Dehapiot,[3] Li Tian,[4] Florence Molinari,[5] Jerome Laurin,[1] François Guillemot,[6] Christian A. Hübner,[7] Christophe Pellegrino[1] and Claudio Rivera[1,2]

Abstract

Although the Na-K-Cl cotransporter (NKCC1) inhibitor bumetanide has prominent positive effects on the pathophysiology of many neurological disorders, the mechanism of action is obscure. Attention for elucidating the role of Nkcc1 has been mainly focused on neurons. Recent single cell mRNA sequencing analysis has demonstrated that the major cellular populations expressing *NKCC1* in the cortex are non-neuronal.

We used a combination of conditional transgenic animals, *in vivo* electrophysiology, two-photon imaging, cognitive behavioral tests and flow cytometry to investigate the role of Nkcc1 inhibition by bumetanide in a mouse model of controlled cortical impact (CCI).

Here, we found that bumetanide rescues parvalbumin-positive interneurons by increasing interneuron-microglia contacts shortly after injury. The longitudinal phenotypic changes of microglia were significantly modified by bumetanide, including an increase in the expression of microglial-derived Bdnf. These effects were accompanied by the prevention of CCI-induced decrease in hippocampal neurogenesis. Treatment with bumetanide during the first week post-CCI resulted in significant recovery of working and episodic memory as well as changes in theta band oscillations one month later.

These results disclose a novel mechanism for the neuroprotective action of bumetanide mediated by an acceleration of microglial activation dynamics that leads to an increase of parvalbumin interneuron survival following CCI, possibly resulting from increased microglial Bdnf expression and contact with interneurons. Salvage of interneurons may normalize ambient gamma-aminobutyric acid (GABA), resulting in the preservation of adult neurogenesis processes as well as contributing to bumetanide-mediated improvement of cognitive performance.

Author affiliations:

1 Aix Marseille Univ, INSERM, INMED, Marseille, France

2 Neuroscience Center, University of Helsinki, Helsinki, Finland

3 Aix Marseille Univ, CNRS, IBDM-UMR7288, Turing Center for Living Systems, Marseille, France

4 Institute of Biomedicine and Translational Medicine, University of Tartu, Tartu, Estonia

5 Aix Marseille Univ, Inserm, MMG, Marseille, France

6 The Francis Crick Institute, 1 Midland Road, London NW1 1AT, UK

7 Institut für Humangenetik, Universitätsklinikum Jena, Jena, Germany

Correspondence to: Claudio Rivera

INMED, INSERM 1249, 163 route de Luminy, 13273 Marseille 09

Neuroscience Center, University of Helsinki, Helsinki, Finland

E-mail: claudio.rivera@helsinki.fi

Running title: Bumetanide acts on inflammation post-TBI

Keywords: traumatic brain injury; microglia; chloride homeostasis; neuroinflammation; GABAergic transmission

Abbreviations: BDNF = Brain-derived neurotrophic factor; CCI = Controlled Cortical Injury; DCX = Doublecortin; DG = Dentate Gyrus; GFAP = Glial Fibrillary Acidic protein; LPS = Lipopolysaccharide; NKCC1 = Sodium Potassium Chloride Cotransporter 1; NOR = Novel Object Recognition; ODT = Object Displacement Task; RGL = Radial Glial-Like cells; PV = Parvalbumin; TBI = Traumatic Brain injury

Introduction

Traumatic brain injury (TBI) is one of the most prevalent pathologies worldwide with more than 20 million people affected each year[1]. However, possibilities for intervention to prevent comorbidities and long-lasting sequelae that frequently follow TBI are limited. Understanding the changes and key players involved in the pathophysiology of the latent phase may help to prevent or reduce some of the comorbidities that accompany TBI.

TBI can be frequently associated with complications such as epileptic seizures, depression and memory impairment[2]. This may partly result from the alteration of hippocampal information processing and neurogenesis[3–5]. However, the mechanisms regulating neurogenesis following TBI remain elusive because of contradictory reports [3,6].

Adult neurogenesis is controlled by local GABAergic interneurons and $GABA_A$ receptors. In particular, the release of GABA by parvalbumin (PV)-expressing interneurons controls the quiescent state of radial glia-like cells (RGL) in the dentate gyrus (DG)[7]. Studies in humans and mouse models of TBI have demonstrated a progressive loss of PV-expressing interneurons in both the ipsi- and the contralesional hippocampus that can persist over months [8–10]. We have previously shown that the inhibition of chloride uptake by bumetanide, an inhibitor of Na-K-Cl (NKCC1) co-transport, significantly decreased PV interneuron loss with a positive effect on both depressive-like behavior and cognitive performance[6]. Despite the potential clinical relevance of these results, the underlying mechanisms remain unknown.

Previous studies on chloride uptake in the brain mainly focused on neuron-intrinsic mechanisms, although the expression of the principal chloride cellular uptake transporter Nkcc1 is mainly expressed in non-neuronal cells[11].

Glial cells are involved early on in the temporal sequence of the neuroinflammatory processes following TBI[12]. Indeed, quiescent glial cells are rapidly activated by a process called "reactive gliosis". The recruitment of peripheral neutrophils is also observed, which is followed by infiltration of lymphocytes and monocyte-derived macrophages. Simultaneously, the release of pro-inflammatory and anti-inflammatory cytokines promotes and/or inhibits the post-traumatic neuroinflammatory response[13]. Activated microglia trigger and maintain astrocytic activation through the release of cytokines, which in turn act on surrounding glial cells and neurons[14]. In

addition, recent reports showed an important pro-survival function of physical contact between activated microglia and interneurons, especially PV-positive interneurons[15].

In this study, we identified a novel mechanism involving cellular chloride uptake in microglia, interneuron survival and neurogenesis that is linked to TBI-induced cognitive decline.

Material and methods

For full description of experimental procedures please see supplementary material and methods.

Experimental Animals

Wild-type mice had a C57bl6-J background. Three transgenic lines were used : Nestin-GFP[16], hGFAP-Cre[17] (line 77.6 mice Stock No. 024098; The Jackson Laboratory) x Nkcc1 flox[18] and B6.129P-Cx3cr1tm1Litt/j[19] and were maintained on a mixed genetic background. All animal experiments complied with the French and Finnish ethical committee approved all experimental procedures (N°: APAFIS#2797 and ESAVI/3183/2022), the ARRIVE guidelines and were carried out in accordance with the U.K. Animals (Scientific Procedures) Act, 1986 and associated guidelines and EU Directive 2010/63/EU for animal experiments.

Controlled-cortical impact (CCI) model

Buprenorphine (0.03 mg/kg) was injected intraperitoneally (IP) into 10-week-old C57bl6-J males 30 minutes before surgery. Mice were then anesthetized using 4% isoflurane mixed with air and enriched with oxygen (0.3 %) and positioned in a stereotaxic frame (David Kopf Instruments®). Body temperature was monitored throughout the procedure using a rectal probe and maintained at 37±2°C with a heating pad (Harvard Apparatus®). A unilateral craniotomy was performed at the level of the right posterior parietal cortex. CCI was performed using a Leica impactor with standardized parameters (tip diameter 3mm, 6 m/sec speed, 1.5 mm depth and 200 msec duration). Animals were allowed to recover on the heating pad before being transferred to a post-surgical room. Before the experiment, animals were randomly assigned to one of the following groups:

sham-vehicle (Sham Veh), sham-bumetanide (Sham Bum), CCI-vehicle (CCI Veh), and CCI-bumetanide (CCI Bum).

Drug delivery

A bumetanide stock solution 20 mM (Sigma-Aldrich®, B3023) was prepared by dissolving 36.4 mg of powder into 1 ml of absolute ethanol. IP injections were performed twice daily 12h apart either during the first week post-CCI at 2 mg/kg or during one-week preceding CCI.

Minocycline (Sigma-Aldrich®, M9511) was injected twice daily, 12h apart (45 mg/kg) for one week. The vehicle solution consisted of the same preparation but lacked the bumetanide/minocycline powder to respect volume and diluent.

Immunohistochemistry

Immunohistochemistry was performed on 4% paraformaldehyde fixed free-floating sections. Incubation with primary antibodies diluted in PBS with 5% NGS and 0.3% Triton X-100 was carried out at 4°C overnight using rabbit anti-doublecortin (ab18723, Abcam, 1:1000), mouse anti-parvalbumin (p3088, Sigma, 1:500), rabbit anti-Iba1 (W1W019-19741, Wako, 1:500), mouse anti-GFAP (MAB360, Merck Millipore, 1:500), mouse anti-BDNF antibody (MAB#918), mouse anti-RFP antibody (MA5-15257, Thermofisher Scientific, 1:500), chicken anti-GFP antibody (AB_2307313, Avès Labs, 1:300) as well as corresponding Alexa Fluor-conjugated secondary antibodies (Thermo Fisher Scientific, 1:500).

PV microglia contact quantification

Confocal stack with double immunofluorescent labeling (Parvalbumin and Iba1) were acquired using a LSM-800 Zeiss confocal microscope Plan Flour 40x/1,30 NA oil immersion objective. Optical sections were collected from the ipsi- and contralesional hippocampi of mice treated and non-treated with bumetanide, at 3 and 7 days post-CCI. Images were then reconstructed in 3D with

Imaris Software. Then contacts between microglia Parvalbumin interneurons were quantified with imageJ® plugin SynapCountJ.

Flow cytometry analysis

Fresh cortical tissues were dissected and gently chopped and minced in 1 mL ice-cold flow cytometry staining buffer (PBS + 1% fetal calf serum) through a 100 µm filter on ice. The homogenates were first blocked in PBS with 10% rat serum with gentle rotation in a cold room and then stained for 1 h protected from light at 4°C with CD206-FITC (cat no. 141704, Biolegend®) + MHCII-PE (cat no. 107608, Biolegend®) + CD11b-PerCP/Cy5.5 (cat no.101228, Biolegend®) + CD45-APC (cat no.103112, Biolegend®). After staining, cells were fixated with 8% PFA for 30 mins, centrifuged at 2000 rpm. Samples were acquired with a 2-laser, 6-color cytometer Gallios (Beckman Coulter®). Gating strategy was determined based on the specific staining of markers for microglial populations[20] .

Live Imaging

Imaging was performed on 5-month-old male mice (B6.129P-Cx3cr1tm1Litt/j, n=5) carrying a cranial window surrounded by a metallic head plate. One month after surgery, trained awake animals were head-fixed on a Mobile HomeCage® platform (MHC V5, Neurotar®) under a custom-built two-photon microscope (Femtonics®) equipped with Mai Tai® Ti:Sapphire Ultrafast Laser (Spectra-Physics) and imaged longitudinally using a Nikon Apo LWD 25X objective with 1.10 numerical aperture for 5 days. An image stack with a 5 mm step size covering 300 mm was acquired. After a 30 min baseline recording, injury was then achieved by focal excitation of 1 cell for 20s at 75 us/pixel at 100% laser intensity. After the injury, animals were treated (Vehicle/Bumetanide) twice per day and imaged, and z-stacks were collected with 5 min intervals for 1 h.

To compute the microglial cell dynamics, we designed a semi-automated procedure using a using Python. Sub-volumes were cropped around each cell before undergoing spatial registrations using pystackreg (G. Lichtner, pystackreg, (2022), https://github.com/glichtner/pystackreg). Cell

dynamics were evaluated from the segmented image by calculating the percentage of binary pixels changing in value from one time point to another [21].

Behavioral tests

One month post-CCI, mice were tested on different tasks using the object recognition paradigm to test the individual components of episodic-like memory, namely the novel object recognition (NOR) and the object displacement task (ODT)[25]. For NOR, mice were placed in the center of a box (Noldus apparatus®, 38.5 cm x 38.5 cm) and allowed to freely explore the space for 10 mins, then two identical objects were added. After a 3 min retention time, one of the objects was replaced and the time of exploration was measured for a 3 min period. The same experiment was also performed with 1 h retention time. A similar protocol was used for ODT with the difference that after the 3 min retention time, one of the objects was moved and the time of exploration of each object was recorded.

Mice were also tested in the Barnes maze (BM) test. One-month post-CCI, mice were trained twice daily for 4 days. On trial probe day (day 5), the target box was replaced with a false escape. The distance travelled, the number of errors, the time spent in the target zone and the latency to reach the target hole were measured.

Finally, mice were tested for anxiety using the elevated plus maze (EPM) test (Ugo Basile company®). For each test, mice were placed in the center square, facing an open arm, and allowed to move freely for 5 min. Entries and time spent in one of the two open or closed arms and center were monitored. Recording and analyses were done using the Ethovision software (Noldus®).

In vivo electrophysiological recordings

Scalp electroencephalographic (EEG) recordings were performed in freely moving mice 3 weeks post-CCI. Telemetric recording electrodes were implanted at the level of the posterior parietal cortex (2 mm posterior to and 1.5 mm left of the bregma). A reference electrode was placed rostral

in the cerebellum. After a 72-hour recovery, EEG (amplified 31,000, filtered at 0.1–120Hz pass, acquired at 1000Hz) was monitored using a telemetric system (Emka Technologies S.A.S) for 3 days, 24 hours per day.

Multisite intrahippocampal recordings were performed by implanting a one shank 16 channels linear probe (A1x16-3mm-100-177, Neuronexus) through a 1mm diameter craniotomy at the posterior parietal level (2 mm posterior, 1.5 mm left of the bregma and 1mm ventral) on head restrained animals trained on Mobile HomeCage® (MHC V5, Neurotar®). Animals were recorded 3 times 10 minutes. Recordings were acquired using the Allego software (SmartBox Pro™, Neuronexus) and a sampling rate of 30K Hz per channel.

For EEG recordings Animal temperature as well as movement were used to determine active and non-active time windows. Delta (1-4 Hz), Theta (4-12 Hz) and Gamma (30-80 Hz) bands[26] were normalized using the ratio of power in the first to the last minute within each recording session. The mean normalized power of active time windows was subtracted from non-active for each recording.

From intrahippocampal recordings individual units were isolated from multisite LFP recordings using Spyking-Circus[27]. The Single-unit activity were further classified into wide-spiking (WS) and narrow-spiking (NS) units[28] based on the spike waveform, autocorrelogram, and cross-correlogram (CCG). NS and WS presumably correspond to putative inhibitory and excitatory units, respectively[29,30].

Statistical Analysis

All mean values are given with the standard error mean (SEM). Normality was tested using a D'Agostino-Pearson test. Two-tailed Student's t tests were used for testing statistical significance between two groups while Mann-Whitney tests were used when the normality test failed. Ordinary one-way ANOVA tests were used to compare three or more groups. In the event that the normality assumption was violated here, the Kruskal-Wallis test was used. When variances were unequal, the Brown-Forsythe ANOVA was used.

Statistics were done using Prism Version 8.3.0 (GraphPad software, Inc., La Jolla, CA, USA) and are represented as follows: * $p < 0.05$; ** $p < 0.01$ and *** $p < 0.001$; all results and statistical significance are reported in Appendix table S1.

Data availability

The data that support the findings of this study are available from the corresponding author, upon reasonable request.

Results

Bumetanide ameliorates CCI-induced memory impairment and pathological neuronal activity

To investigate the effects of bumetanide on post-TBI cognitive behavior, we performed four cognitive performance tests: the Novel Object Recognition (NOR) and the Object Displacement Task (ODT). CCI induced a significant decrease in the recognition ratio of the tasks examined after normalization to Sham conditions unless otherwise stated (ODT: CCI Veh 0.38 ±0.06; NOR 5 mins: CCI Veh 0.44 ±0.20; NOR 1 h Sham 1.17 ±0.58 vs CCI Veh 0.507 ±0.31, Fig 1B, C and D). Interestingly, the strongest effect of bumetanide was found in NOR with 1 h retention (CCI Bum 0.86 ±0.40, Fig 1D). We then used a spatial memory test, the Barnes Maze (BM), which showed that CCI induced a significant increase of the latency in reaching the target hole (Sham 8.00 ±0.58 vs CCI Veh 44.00 ±7.61, Fig 1E). Similarly, bumetanide treatment resulted in a better performance compared to vehicle (CCI Bum 13.00 ±1.95, Fig 1E). Finally, as NOR and ODT are strongly influenced by anxiety, we used the Elevated Plus Maze (EPM) to test this parameter and did not find significant differences in the number of entries that animals made into each zone (Center: Sham 40.00 ±0.58 vs CCI Veh 44.00 ±4.02 vs CCI Bum 41.40 ±3.11; Open arms: Sham 35.33 ±2.186 vs CCI Veh 35.00 ±6.18 vs CCI Bum 46.00 ±1.86; Closed arms: Sham 65.33 ±10.11 vs CCI Veh 79.75 ±10.82 vs CCI Bum 58.00 ±12.03) (Fig 1F). There were also no differences in the time that animals spent in the center (Sham 51.18 ±1.657 vs CCI Veh 35.00 ±5.343 vs CCI Bum 43.048 ±5.306), nor in the open arms (Sham 82.44 ±18.79 vs CCI Veh 100.70 ±23.10 vs CCI Bum

71.98 ±12.39), nor in the closed arms (Sham 145.72 ±9.97 vs CCI Veh 151.96 ±18.27 vs CCI Bum 176.264 ±8.27) (Fig 1G). These results show that CCI has a negative impact on learning performance and spatial memory, that it is not linked with anxiety.

Memory impairment following TBI are characterized by changes in theta rhythms [31,32,33]. Using telemetric EEG, we found that at 1-month post-CCI, the power of theta band oscillations in vehicle treated animals was significantly lower compared to sham (Sham 6.50 % ±0.18 vs CCI Veh 3.42 % ±0.41, Fig 1I). Bumetanide treatment normalized the theta band power and was significantly different from vehicle treated animals (CCI Bum 6.14 % ±0.29, Fig 1I). The power of the delta band was lower in CCI animals and was not affected by bumetanide treatment (Sham 5.44 % ±0.18 vs CCI Veh 1,14 % ±0,17 vs CCI Bum 1.82 % ±0.53, Fig 1H). Similarly, the power of the gamma band was significantly higher in vehicle-treated animals compared to sham but not changed in bumetanide animals (Sham 0.39 % ±0,03 vs CCI Veh 0.89 % ±0,13 vs CCI Bum 0,70% ±0.08, Fig 1J). To assess the impact on single-unit activity we isolated putative interneuron and principal neuron single-units from intrahippocampal multisite recordings. Here we found that the spike rate of putative interneurons was significantly decreased in vehicle compared to Sham animals (Sham 23,38 ±2,42 Hz vs CCI Veh 3,26 ±0,6824 Hz) but not in bumetanide animals (Bum 15,08 ±2,274 Hz; Fig 1K). Interestingly, putative principal cell unit spike rate was not affected in all groups (Fig 1L). The number of total recorded putative interneurons was much lower in Vehicle (5) animals than Sham (10) and Bumetanide (12) treated whereas principal cell number was constant in all conditions (Sham: 47 cells; Veh:48 cells; Bum:48 cells; Fig 1M). These results suggest that bumetanide ameliorates CCI-induced changes in interneuron function.

Bumetanide rescues CCI-induced changes in secondary neurogenesis and PV interneuron loss

Interneurons are important contributors to brain oscillations[34]. PV-positive interneurons are a particularly vulnerable subpopulation following CCI[7]. In addition, the impact of CCI on interneuron activity and reduction in numbers suggest changes in the interneuron population of the hippocampus following CCI. We quantified PV-positive interneurons in the granular layer of the

ipsi- and contralesional DG during the first post-traumatic week at 3 and 7 days post-CCI (dpCCI). Both sides showed a significant reduction in the number of PV interneurons at 3 dpCCI (normalized value on sham: sham contra 1.00 ±0.20 vs contra Veh 0.52 ±0.18 and sham ipsi 1.00 ±0.22 vs ipsi Veh 0.22 ±0.18, Figs 2A and B). This loss was significantly reduced by bumetanide treatment in the contra- (0.77 ±0.23) and ipsilesional side (0.51 ±0.14, Fig 2A and B). We also found a significant reduction in the PV-containing interneurons survival at 7 dpCCI in both sides (normalized value on sham: sham contra 1.0 ±0.27 vs contra Veh 0.59 ±0.18 and sham ipsi 1.00 ±0.27 vs ipsi Veh 0.14 ±0.12, Fig 2C and D). This loss was significantly reduced at the contra- (1.02 ±0.34) and ipsilesional sides (0.71 ±0.24, Fig 2C and D) by bumetanide treatment. Bumetanide-induced interneuron survival was not restricted to the DG, as we found a similar effect on other hippocampal regions (in ipsilesional CA3: Sham 1.00 ±0.12 vs Ipsi Veh 0.52 ±0.09; and in ipsilesional CA1: Sham 1.00 ±0.25 vs Ipsi Veh 0.37 ±0.07).

Ambient GABA, provided by the ongoing activity of DG interneurons and particularly PV interneurons, plays a role in the proliferation and migration of granular cell progenitors [6,35]. A loss of PV interneurons may significantly contribute to the TBI-induced changes in stem cell proliferation by reducing GABA release. At 7 dpCCI, we observed a significant reduction in the number of DCX-positive neurons within both the ipsi- and contralesional DG (normalized value on sham: sham ipsi 1.00 ±0.31 vs. CCI Veh ipsi 0.19 ±0.09 and sham contra 1.00 ±0.31 vs. CCI Veh contra 0.78 ±0.24, Figs 2E, F, H and I). This coincided with an increase in the number of Nestin-positive cells within the DG (sham ipsi 1.00 ±0.17 vs. CCI Veh ipsi 2.08 ±0.29 and sham contra 1.00 ±0.18 vs. CCI Veh contra 1.37 ±0.34 Figs 2E, G, H and J). Bumetanide treatment reduced the number of Nestin-positive cells (CCI Bum ipsi 1.4 ±0.24 and CCI Bum contra 1.0 ±0.15, Figs 3E, G, H and J) and triggered an increase in the number of DCX-positive cells (CCI Bum ipsi 0.47 ±0.16 and CCI Bum contra 0.98 ±0.23, Figs 2E, F, H and I).

Bumetanide rescues CCI-induced changes in microglia morphology/phenotype and increases contacts with PV interneurons

Neuroinflammation is present in the primary (acute) and secondary (chronic) stages of TBI[12] where microglia and astrocyte activation are involved in the mechanisms leading to both adverse and

beneficial effects. Under physiological conditions Nkcc1 is predominantly expressed in astrocytes and microglia compared to neurons[36]. Therefore, we wondered whether these cell populations contribute to the effect of bumetanide. This was monitored in GFAP-Nkcc1-KO mice. Although we observed an abnormal morphology of astrocytes in this transgenic line, we did not find a significant increase in interneuron survival following CCI, suggesting that astrocytic chloride homeostasis is not relevant in CCI-induced apoptosis. (See full description in Supplementary Results and Fig. S1).

TBI is known to induce a strong inflammatory reaction[37]. To see if TBI-induced effects on PV survival and proliferation are sensitive to microglial activation, we used the anti-inflammatory drug minocycline. Interestingly, treatment with this agent resulted in similar effects on both PV survival (Contra Veh 0.59 ±0.18 vs Contra Mino 1.21 ±0.34 and ipsilesional side Ipsi Veh 0.14 ±0.12 vs Ipsi Mino 0.74 ±0.39, Fig 2A, B, C and D) and newborn neurons (CCI Mino ipsi 0.63 ±0.17 and CCI Mino contra 1.12 ±0.10, Fig 2E, F, G and H). These results suggest that microglia activation affect post-CCI interneuron survival and adult born neuron production.

To investigate whether the effect of bumetanide depends on Nkcc1 in microglia, we used a transgenic approach for Tamoxifen (Tam) inducible knock-down of Nkcc1 in CX3CR1-positive microglia. Here, we observed that bumetanide treatment induced a significant increase in the average cell size in the control condition (Tam + Bum 105732 µm² ±18324 vs ShNKCC1 + RFP 27650 µm² ±4322 vs Tam + RFP 17482 µm² ±2164). Interestingly, knockdown of Nkcc1 also induced an increase in size (Tam + ShNKCC1 + RFP 127090 µm² ±29570 vs ShNkcc1 + RFP 27650 µm² ±4322 vs Tam + RFP 17482 µm² ±2164) (Fig 3A and C). Similar results were found in BV2 cells (Fig S2). Then, we investigated the phagocytosis capacity of the cells in the different conditions. Bumetanide treatment induced a significant increase in the number of engulfed beads (Tam + Bum 28.00 ±6.66 vs ShNkcc1 + RFP 9.34 ±3.45 vs Tam + RFP 6.08 ±3.64). Knockdown of Nkcc1 had similar effect (Tam + ShNkcc1 + RFP 25.46 ±3.58 vs ShNkcc1+ RFP 9.34 ±3.45 vs Tam + RFP 6.08 ±3.64) (Fig 3B and C). These results suggest that bumetanide can regulate microglia morphology and activation by modulating Nkcc1 activity.

Furthermore, bumetanide treatment *in vivo* induced a significant increase of microglia endpoint numbers (Sham 715.9 ±81.03 vs CCI Veh 698.8 ±331.2 vs CCI Bum 1076.0 ±85.13), number of attachment points (Sham 41.86 ±12.40 vs CCI Veh 101.9 ±43.70 vs CCI Bum 140.8 ±54.96) and

soma area (Sham 1458 µm² ±652.7 vs CCI Veh 3494 µm² ±757.6 vs CCI Bum 4985 µm² ±850,6) (Fig 4A and B) in the ipsilesional DG 3 dpCCI.

Microglia process motility and their interactions with interneurons play an important role in PV survival[38]. We found significant differences in the number of contacts between microglial cells and PV interneurons between vehicle and bumetanide-treated animals at 3 dpCCI in both the contra- (CCI Veh 40.00 ±24.92 vs CCI Bum 103.50 ±23.55) and ipsilesional side (CCI Veh 2.75 ±2.48 vs CCI Bum 63.20 ±9.04) (Fig 4C and D). In addition, there was no significant difference between Sham and CCI Bum in the contralesional side (Sham contra 115.9 ±13.50 vs CCI Bum contra 93 ±12.48) but a slight difference in the ipsilesional side (Sham ipsi 99.57 ±13.01 vs CCI Bum ipsi 63.20 ±9.04) (Fig 4C and D).

Using flow cytometry, we found that microglia were more likely to express the pro-inflammatory markers CD45, MHCII and CD172a (Veh $MHCII^{+}$ 13.55 % ±4.91 vs Bum $MHCII^{+}$ 21.59 % ±6.03; Fig 4E and F) after 3 days of bumetanide treatment. To confirm this, we measured interleukins in brain tissue and found a significant increase in IL-6 in the hippocampus of CCI animals treated with bumetanide (CCI Bum 21.94 pg/mL ±6.03 vs Sham 11.49 pg/mL ±0.91 and CCI Veh 12.85 pg/mL ±3.89, Fig 4G). Since TBI is characterized by inflammatory cell infiltration promoted by opening of the blood brain barrier (BBB), we also looked at blood cells. The $CD45^{high}$-$CD11^{low}$ cells (e.g., possibly lymphocytes) were few in our samples and included not only neutrophils but also other innate immune cells (e.g., monocytes, macrophages and DCs) as reported in the second gating plot of Figure 4E. However, systemic inflammation is not influenced by IP bumetanide treatment, while intracortical inflammation is reduced by the same treatment[39]. Thus, it is plausible that the effects of bumetanide may result from resident microglial cells and not infiltrating cells.

At 7 dpCCI, we found less prominent morphological changes in microglia cells with no effect of bumetanide in both the ipsi- and contralateral side: a decrease in the number of endpoints (Sham 900.7 ±167.9 vs CCI Veh 696.5 ±86.72 vs CCI Bum 659 ± 100.4) and of process length (Sham 256.7 µm ±46.75 vs CCI Veh 197.8 µm ±17.17 vs CCI Bum 192.7 µm ±42.21) (Fig 5A and B). Despite this, the number of contacts between microglial cells and PV interneurons still differed for the ipsilesional side (CCI Veh 25.20 ±12.30 vs CCI Bum 39.56 ±5.85), without difference between Sham and CCI Bum (Sham ipsi 57 ±6.382 vs CCI Bum ipsi 41.23 ±2.472) (Fig 5C and D). Surprisingly, bumetanide promoted the expression of the pro-phagocytosis marker CD206 by

microglia (Veh $CD206^+$ 16.79 % ±2.957 vs Bum $CD206^+$ 27.44 % ±8.635, Fig 5E and F). In line with these results, we also found a significant increase of interleukin 10 (IL-10) expression in CCI animals treated with bumetanide compared to control and vehicle-treated animals (CCI Bum 5.32 pg/mL ±0.86 vs Sham 1.69 pg/mL ±0.78 and CCI Veh 2.57 pg/mL ±0.65, Fig 5G).

These results suggest that bumetanide protects PV interneurons by increasing microglia contacts during the first post-traumatic week as well as by regulation of microglia phenotypes. This allows us to postulate that bumetanide treatment protects PV interneurons through anti-inflammatory and pro-survival mechanisms mediated by microglia.

Bumetanide increases microglia Bdnf expression

Microglia are a central source of Bdnf, an important neurotrophin controlling neuronal survival and plasticity[40–42]. Therefore, we measured the level of BDNF expression in microglial-like BV2 cells after 24 and 72h of treatment. 24 hours of bumetanide treatment led to a significant increase of Bdnf levels (Ctrl 0.18 pg/mL ±0.02 vs Bum 2.79 pg/mL ±0.18, Fig S2H; Fig S2H). This effect was attenuated but still present after 72h of treatment (Ctrl 0.19 pg/mL ±0.03 vs Bum 0.31 ±0.14, Fig S2I). In addition, we quantified the immuno-like intensity of Bdnf in sham vehicle, sham bumetanide, CCI vehicle and CCI bumetanide treated animals and found a consistent increase in Bdnf expression within Iba1-positive microglia in bumetanide-treated animals either on the contralesional (normalized value on sham vehicle : Sham Veh 1.00 ±0.12 vs Sham Bum 3.55 ±0.30 vs CCI Veh 2.27 ±0,41 vs CCI Bum 5.60 ±0.75) or the ipsilesional side (normalized value on sham vehicle : Sham Veh 1.00 ±0.06 vs Sham Bum 4.28 ±0.20 vs CCI Veh 3.28 ±0.18 vs CCI Bum 12,86 ±1.06; Fig 5G, H and I). These results indicate that bumetanide induces Bdnf expression, which may play an important role in the survival of PV interneurons.

Bumetanide regulates post-CCI microglia process motility

To further investigate microglia *in vivo*, we performed longitudinal 2-photon imaging in $Cx3CR1^{+/GFP}$ mice following laser-induced injury on the posterior parietal cortex (see supplementary information for a full description of the procedure). Quantification of microglial process length and motility during the first week post-injury revealed that bumetanide induced a

significant decrease in process length one day post-laser injury. This difference was not significant 5 dpCCI (Veh Day 1 33.58 ±3.66 vs Bum Day 1 24.43 ±1.37; Veh Day 5 ±3.69 vs Bum Day 5 42.51 ±2.23; Fig 6B, D and C). Interestingly, bumetanide induced a significant decrease in the motility ratio at both 1- and 5-dpCCI (Veh Day 1 0.59 ±0.1 vs Bum Day 1 0.52 ±0.01; Veh Day 5 0.70 ±0.03 vs Bum Day 5 0.61 ±0.12, Fig 6B, D and E). These experiments are in line with the effect of bumetanide on process length in CCI animals, and a decreased motility ratio is consistent with the increased number of contacts between microglia and PV interneurons.

The effect of bumetanide is physiological state dependent

Brain injury is paradoxically aggravated in microglia NKCC1-deficient mice[39]. As under these conditions chloride uptake is impaired prior to the trauma we asked if bumetanide treatment prior to CCI would have a different effect than when administered after CCI. Interestingly, administration of bumetanide during one week before CCI worsened CCI outcomes and, more particularly, PV survival. Indeed, bumetanide-treated animals showed a significant decrease of PV interneurons compared to Sham and vehicle treated animals on the ipsilesional side (normalized value on sham: Sham 1 ± 0.05 vs CCI Veh 0.54 ±0.09 vs CCI Bum 0.10 ±0.02) and compared to Sham on the contralesional side (normalized value on sham: Sham 1 ±0.05 vs CCI Veh 0.90 ±0.12 vs CCI Bum 0.57 ±0.12) (Fig 7A and B). These results indicate that the impact of bumetanide on PV-interneuron survival is dependent of the physiological state and the mechanism disclosed in this study is mainly relevant under pathological conditions.

Discussion

How cognitive deficits observed in experimental models and clinical TBI develop following an initial concussion is not well understood[5]. In this study, we were interested how chloride homeostasis might be involved in post-traumatic changes in working memory[43]. Theta rhythm is a potential electrophysiological biomarker of altered neuronal activity[44,45] and is believed to synchronize activity both within local networks and between distal cortical regions involved in cognitive processing[46,47]. In both humans and rats, the power of theta rhythm increases during the acquisition phase of spatial learning and object recognition. Treatment- or injury-induced inhibition

of theta oscillations correlates with cognitive dysfunction[32,48,49]. In agreement, we found a positive correlation between decreased theta-band power and poor performance in the spatial cognitive test after one-month post-CCI. Interestingly, we found that an early transient treatment with the chloride cellular uptake inhibitor bumetanide was effective to counteract the long-term changes in both behavior and theta oscillations.

Several studies link cognitive processes with normal adult neurogenesis in the hippocampus. This corresponds with the generation of functional neurons from adult neural stem cells. TBI can induce significant changes in the proliferation and maturation of granular cells[50,51]. In the present study we found a significant increase in the number of Nestin-positive cells in both ipsi- and contralesional DG of mice 7 dpCCI. Nestin is a radial glia (RGL) cell marker, and represents a pool of quiescent cells that divide only occasionally[16]. The division of these RGLs leads to the generation of intermediate progenitor cells (IPCs) that will undergo a limited number of rapid divisions before entering the neuronal differentiation pathway[52]. IPCs are divided into two subtypes: i) type 2a cells that are positive for Nestin and negative for double-cortin (DCX), an immature neuronal marker, and ii) type 2b cells, positive for Nestin and DCX[53]. IPCs then give rise to neuroblasts (type 3 cells), which express DCX[54] . The increased number of Nestin-positive cells after TBI might intuitively suggest that there will be an increase in the number of newborn neurons. This is, however, not the case since we found a significant decrease of DCX positive cells in both the contra- and ipsilesional side of the DG. These results indicate that TBI leads to an increase in the quiescent cell pool and a resulting decrease in the number of immature granule cells consistent with previous findings[6]. Furthermore, treatment with bumetanide during the first week post-TBI significantly reduced the CCI-induced decrease in Nestin-positive cells, as well as increased the number of DCX-positive cells. These results suggest that the effects of bumetanide on cognitive performance could be related to positive effects on post-traumatic granule cell production. In addition, they may suggest a common upstream mechanism for the action of bumetanide.

GABA, especially released by PV interneurons[7,55], appears to play a central role in regulating the activity of RGLs by inhibiting their proliferation. Thus, post-traumatic changes in granule cells could be related to abnormal interneuron function. Indeed, we found loss of PV interneurons in the granular layer of the hippocampus, as early as 3 dpCCI in both the ipsi- and contralesional side that

was sustained at 7 dpCCI and one month after trauma[6]. This loss of PV interneurons may also contribute to abnormal brain activity in TBI[56].

The increase of Nestin-positive cells and decrease in DCX cells that we detected after TBI can thus be related to the loss of PV interneurons, which results in less ambient GABA[57,58] . In accordance with this assumption, treatment with bumetanide significantly counteracted the loss of PV interneurons and normalized the CCI induced change in Nestin and DCX positive cells. As these cell populations were not significantly affected in sham animals by bumetanide a direct effect on progenitors may have less prominent importance.

Neuroinflammation is observed in both the acute and chronic stages of TBI[12]. It appears to be responsible for both detrimental and beneficial effects by contributing to primary injury and secondary damage, but also facilitating tissue repair[59]. Both astrocytes and microglia are important players in the mechanisms of brain inflammation and, in addition, display one of the highest expression levels of Nkcc1 in the brain. Thus, it is plausible that the post-traumatic effects produced of bumetanide could be related to an influence on the dynamics of inflammatory processes[59,60].

Following this idea, we first studied the role of Nkcc1-mediated chloride uptake in astrocytes using conditional transgenic animals. Despite bumetanide having substantial effects on the morphology of GFAP-positive cells in both the contra- and ipsilateral sides in sham animals, the ablation of Nkcc1 in these cells did not rescue the loss of PV-positive interneurons. This indicates that astrocytes are not significantly involved in the bumetanide-induced increase in interneuron survival. Nevertheless, in this study we only monitored the first week post-CCI and we cannot exclude effects at more delayed stages of injury.

To define if CCI induced neuroinflammation through microglia could influence PV interneuron survival we first treated animals with minocycline, a second-generation tetracycline derivative that has an anti-inflammatory and neuroprotective action. Minocycline is known to have anti-inflammatory effect via the inhibition of microglial cells activation[61] and induce microglial Bdnf expression[62]. Minocycline increased the survival of interneurons and the number of newborn neurons, suggesting that microglia inflammation is involved.

Interestingly, bumetanide treatment induced phenotypic changes in microglia and lead to a faster activation of microglial cells into a pro-inflammatory phenotype at early stages, which is required for cell debris removal and phagocytosis of apoptotic cells. At 7 dpCCI, microglial cells of

bumetanide-treated animals acquired pro-phagocytotic characteristics. Microglia in control animals acquired pro-inflammatory characteristics slightly later, but importantly it persisted more than 7 dpCCI, resulting in a deleterious inflammatory state. Intriguingly, bumetanide increased the concentration of interleukin 6 (IL-6) 3 dpCCI in line with a recent study using the same trauma model showing that hippocampal granule cells derived release of IL-6 is triggered by renewed microglial cells. This increase in neuronal survival, allows adult neurogenesis to proceed normally and prevents behavioral deficits[63]. One-week post-CCI, we detected higher levels of IL-10 in bumetanide-treated animals, along with a phenotype switch. Expression of IL-10 can promote neuronal and glial cell survival and dampen inflammatory responses via a number of signaling pathways[64]. To further investigate if chloride uptake is important for microglia function, we knocked down the expression of Nkcc1 in primary microglia. We observed identical morphological changes and the same higher phagocytosis activity. This is interesting as microglia mediated phagocytosis is important for recovery as well as clearance of degenerated cells[65]. Inhibition of phagocytosis can lead to increase neuronal damage and decrease neuronal cell viability[66].

In addition, we found that bumetanide treatment leads to more contact sites between microglia and PV interneurons *in vivo*. This is consistent with previous results showing pro-survival signaling mediated by microglia contacts on interneurons[15]. These results imply that the mechanism by which bumetanide rescues PV interneurons can be related to additional effects on microglia morphology. In accordance, bumetanide treatment leads to a significant increase of microglia processes and ramifications 3 dpCCI. Moreover, it also significantly changes microglia process motility *in vivo.*

The neurotrophic factor Bdnf is crucial for post-traumatic neuronal survival and plays a central role in microglia sensitive learning paradigms[67,68] as well as microglia modulation of post-traumatic network function[42]. Interestingly, we found here a significant increase of Bdnf in microglia induced by bumetanide following CCI. There is a complex interplay between neurotrophic signaling and chloride homeostasis in neurons e.g Bdnf can normalize post-traumatic $GABA_A$ mediated responses from depolarizing and hyper excitable to hyperpolarizing but have the opposite effect under physiological conditions. This could contribute to neuronal survival under pathological conditions[69,70]. Thus, changes in GABAergic transmission in combination with increased Bdnf release from microglia and increased contact between microglia and interneurons could contribute to bumetanide induced increased survival of PV interneurons.

The effects observed here suggest that bumetanide directly acts on microglia. Indeed, recent work by Tóth *et al*[39] using microglia Nkcc1 deficient mice are in agreement with our results. In addition, they showed that systemic application of bumetanide had positive post-traumatic effects. In contrast, deletion of Nkcc1 in microglia resulted in more severe tissue damage after ischemic stroke. Although these effects are compelling and indicate complicated actions of bumetanide, they do not provide a mechanistic view on the post-traumatic benefits of bumetanide. Moreover, Tóth *et al* disrupted chloride uptake before induction of ischemia. We obtained similar results, when we administered bumetanide already before induction of TBI. Thus, these results show a complex and context dependent effect of bumetanide and indicate that the mechanism disclosed in this study may apply to post-traumatic conditions.

Some limitations of this study could be addressed in future research. For example, we only used males[71–73] and, as previously described[74,75], there are likely sex differences in clinical outcomes after TBI. On the other hand, no significant differences between males and females in lesion volume, neurodegeneration, blood-brain barrier (BBB) alteration and microglia activation have been found in animal models[76,77]. A second potential limitation is that we did not fully study the infiltrating immune cells due to the limited sample size. However, it would be interesting to address this, either as in Tóth *et al*[39] by using specific markers e.g. CD3, CD20 and Ly-6G, or by using transgenic mice like CX3CR1creERT2 x iDTR as in Willis *et al*[63].

In conclusion, this study shows that a treatment targeting inhibition of the chloride co-transporter Nkcc1 can regulate the activation kinetics of microglia and provides a mechanistic link for the positive effect of bumetanide on post-traumatic cognitive decline. These results also open an additional avenue to better understand chloride uptake dependent pathophysiological mechanisms in the post-traumatic brain as well as to identify the elements involved in the development of long-term sequelae following TBI.

Acknowledgements

We thank Prof Eero Castren and Yves-Alain Barde for providing the BDNF antibody. We also thank dr. Tristen Hewitt for comment on the manuscript.

Funding

This work was supported by public Aix-Marseille Université (AMU); Eranet Neuron III program through the Acrobat, ANR GABGANG project and Academy of Finland project nr 341361 through CR; and by the "fondation des gueules cassées" 83-2020 through MT

CAH was funded by grants of the BMBF (01EW1706) and the DFG (HU 800/10-1).

Competing interests

Authors report no conflict of interest.

Supplementary material

Supplementary material is available at *Brain* online.

References

1. GBD 2016 Traumatic Brain Injury and Spinal Cord Injury Collaborators. Global, regional, and national burden of traumatic brain injury and spinal cord injury, 1990-2016: a systematic analysis for the Global Burden of Disease Study 2016. Lancet Neurol 2019;18(1):56–87.
2. Nicholl J, LaFrance WC. Neuropsychiatric sequelae of traumatic brain injury. Semin Neurol 2009;29(3):247–255.
3. Wang X, Gao X, Michalski S, et al. Traumatic Brain Injury Severity Affects Neurogenesis in Adult Mouse Hippocampus. J. Neurotrauma 2016;33(8):721–733.
4. Zheng W, ZhuGe Q, Zhong M, et al. Neurogenesis in adult human brain after traumatic brain injury. J. Neurotrauma 2013;30(22):1872–1880.
5. Graham DI, Adams JH, Nicoll JA, et al. The nature, distribution and causes of traumatic brain injury. Brain Pathol. 1995;5(4):397–406.
6. Goubert E, Altvater M, Rovira M-N, et al. Bumetanide Prevents Brain Trauma-Induced Depressive-Like Behavior. Front Mol Neurosci 2019;12:12.
7. Song J, Zhong C, Bonaguidi MA, et al. Neuronal circuitry mechanism regulating adult quiescent neural stem-cell fate decision. Nature 2012;489(7414):150–154.
8. Santhakumar V, Ratzliff AD, Jeng J, et al. Long-term hyperexcitability in the hippocampus after experimental head trauma. Ann. Neurol. 2001;50(6):708–717.
9. Schiavone S, Neri M, Trabace L, Turillazzi E. The NADPH oxidase NOX2 mediates loss of parvalbumin interneurons in traumatic brain injury: human autoptic immunohistochemical evidence. Sci Rep 2017;7(1):8752.
10. Toth Z, Hollrigel GS, Gorcs T, Soltesz I. Instantaneous perturbation of dentate interneuronal networks by a pressure wave-transient delivered to the neocortex. J. Neurosci. 1997;17(21):8106–8117.
11. Glushakova OY, Johnson D, Hayes RL. Delayed increases in microvascular pathology after experimental traumatic brain injury are associated with prolonged inflammation, blood-brain barrier disruption, and progressive white matter damage. J Neurotrauma 2014;31(13):1180–1193.
12. Lozano D, Gonzales-Portillo GS, Acosta S, et al. Neuroinflammatory responses to traumatic brain injury: etiology, clinical consequences, and therapeutic opportunities. Neuropsychiatr Dis Treat 2015;11:97–106.

13. Aguzzi A, Barres BA, Bennett ML. Microglia: scapegoat, saboteur, or something else? Science 2013;339(6116):156–161.

14. Morganti-Kossmann MC, Rancan M, Otto VI, et al. Role of cerebral inflammation after traumatic brain injury: a revisited concept. Shock 2001;16(3):165–177.

15. Cserép C, Pósfai B, Lénárt N, et al. Microglia monitor and protect neuronal function through specialized somatic purinergic junctions. Science 2020;367(6477):528–537.

16. Mignone JL, Kukekov V, Chiang A-S, et al. Neural stem and progenitor cells in nestin-GFP transgenic mice. J. Comp. Neurol. 2004;469(3):311–324.

17. Gregorian C, Nakashima J, Le Belle J, et al. Pten deletion in adult neural stem/progenitor cells enhances constitutive neurogenesis. J Neurosci 2009;29(6):1874–1886.

18. Antoine MW, Hübner CA, Arezzo JC, Hébert JM. A causative link between inner ear defects and long-term striatal dysfunction. Science 2013;341(6150):1120–1123.

19. Yona S, Kim K-W, Wolf Y, et al. Fate mapping reveals origins and dynamics of monocytes and tissue macrophages under homeostasis. Immunity 2013;38(1):79–91.

20. Li Z, Ma L, Kulesskaya N, et al. Microglia are polarized to M1 type in high-anxiety inbred mice in response to lipopolysaccharide challenge. Brain Behav Immun 2014;38:237–248.

21. Thévenaz P, Ruttimann UE, Unser M. A pyramid approach to subpixel registration based on intensity. IEEE Trans Image Process 1998;7(1):27–41.

22. Young SZ, Taylor MM, Wu S, et al. NKCC1 knockdown decreases neuron production through GABA(A)-regulated neural progenitor proliferation and delays dendrite development. J Neurosci 2012;32(39):13630–13638.

23. Dai X, Li N, Yu L, et al. Activation of BV2 microglia by lipopolysaccharide triggers an inflammatory reaction in PC12 cell apoptosis through a toll-like receptor 4-dependent pathway. Cell Stress Chaperones 2015;20(2):321–331.

24. Giulian D, Baker TJ. Characterization of ameboid microglia isolated from developing mammalian brain. J Neurosci 1986;6(8):2163–2178.

25. Inostroza M, Brotons-Mas JR, Laurent F, et al. Specific impairment of "what-where-when" episodic-like memory in experimental models of temporal lobe epilepsy. J. Neurosci. 2013;33(45):17749–17762.

26. Cohen MX. Analyzing Neural Time Series Data: Theory and Practice [Internet]. 2014.[cited 2022 Nov 21] Available from: https://direct.mit.edu/books/book/4013/Analyzing-Neural-Time-Series-DataTheory-and

27. Yger P, Spampinato GL, Esposito E, et al. A spike sorting toolbox for up to thousands of electrodes validated with ground truth recordings in vitro and in vivo. eLife [date unknown];7:e34518.

28. Watson BO, Levenstein D, Greene JP, et al. Network homeostasis and state dynamics of neocortical sleep. Neuron 2016;90(4):839–852.

29. Csicsvari J, Hirase H, Czurko A, Buzsáki G. Reliability and state dependence of pyramidal cell-interneuron synapses in the hippocampus: an ensemble approach in the behaving rat. Neuron 1998;21(1):179–189.

30. Sirota A, Montgomery S, Fujisawa S, et al. Entrainment of neocortical neurons and gamma oscillations by the hippocampal theta rhythm. Neuron 2008;60(4):683–697.

31. Fedor M, Berman RF, Muizelaar JP, Lyeth BG. Hippocampal θ dysfunction after lateral fluid percussion injury. J. Neurotrauma 2010;27(9):1605–1615.

32. Winson J. Loss of hippocampal theta rhythm results in spatial memory deficit in the rat. Science 1978;201(4351):160–163.

33. Bragin A, Li L, Almajano J, et al. Pathologic electrographic changes after experimental traumatic brain injury. Epilepsia 2016;57(5):735–745.

34. Moxon KA, Shahlaie K, Girgis F, et al. From adagio to allegretto: The changing tempo of theta frequencies in epilepsy and its relation to interneuron function. Neurobiol Dis 2019;129:169–181.

35. Duan X, Kang E, Liu CY, et al. Development of neural stem cell in the adult brain. Curr Opin Neurobiol 2008;18(1):108–115.

36. Hammond TR, Dufort C, Dissing-Olesen L, et al. Single-Cell RNA Sequencing of Microglia throughout the Mouse Lifespan and in the Injured Brain Reveals Complex Cell-State Changes. Immunity 2019;50(1):253-271.e6.

37. Simon DW, McGeachy MJ, Bayır H, et al. The far-reaching scope of neuroinflammation after traumatic brain injury. Nat Rev Neurol 2017;13(3):171–191.

38. Cserép C, Pósfai B, Orsolits B, et al. Microglia monitor and protect neuronal function via specialized somatic purinergic junctions [Internet]. 2019.[cited 2021 Sep 23] Available from: https://www.biorxiv.org/content/10.1101/606079v1

39. Tóth K, Lénárt N, Berki P, et al. The NKCC1 ion transporter modulates microglial phenotype and inflammatory response to brain injury in a cell-autonomous manner. PLoS Biol 2022;20(1):e3001526.

40. Ferrini F, De Koninck Y. Microglia control neuronal network excitability via BDNF signalling. Neural Plast 2013;2013:429815.

41. Lima Giacobbo B, Doorduin J, Klein HC, et al. Brain-Derived Neurotrophic Factor in Brain Disorders: Focus on Neuroinflammation. Mol Neurobiol 2019;56(5):3295–3312.

42. Coull JAM, Beggs S, Boudreau D, et al. BDNF from microglia causes the shift in neuronal anion gradient underlying neuropathic pain. Nature 2005;438(7070):1017–1021.

43. Kent PL. Working Memory: A Selective Review. Appl Neuropsychol Child 2016;5(3):163–172.

44. Buzsáki G. Theta rhythm of navigation: link between path integration and landmark navigation, episodic and semantic memory. Hippocampus 2005;15(7):827–840.

45. Vertes RP. Hippocampal theta rhythm: a tag for short-term memory. Hippocampus 2005;15(7):923–935.

46. O'Neill P-K, Gordon JA, Sigurdsson T. Theta Oscillations in the Medial Prefrontal Cortex Are Modulated by Spatial Working Memory and Synchronize with the Hippocampus through Its Ventral Subregion. J Neurosci 2013;33(35):14211–14224.

47. Ward LM. Synchronous neural oscillations and cognitive processes. Trends Cogn Sci 2003;7(12):553–559.

48. Paterno R, Metheny H, Xiong G, et al. Mild Traumatic Brain Injury Decreases Broadband Power in Area CA1. J Neurotrauma 2016;33(17):1645–1649.

49. Pevzner A, Izadi A, Lee DJ, et al. Making Waves in the Brain: What Are Oscillations, and Why Modulating Them Makes Sense for Brain Injury. Front Syst Neurosci 2016;10:30.

50. Tunc-Ozcan E, Peng C-Y, Zhu Y, et al. Activating newborn neurons suppresses depression and anxiety-like behaviors. Nat Commun 2019;10(1):3768.

51. Gao X, Enikolopov G, Chen J. Moderate traumatic brain injury promotes proliferation of quiescent neural progenitors in the adult hippocampus. Exp Neurol 2009;219(2):516–523.

52. Ming G-L, Song H. Adult neurogenesis in the mammalian brain: significant answers and significant questions. Neuron 2011;70(4):687–702.

53. Kronenberg G, Reuter K, Steiner B, et al. Subpopulations of proliferating cells of the adult hippocampus respond differently to physiologic neurogenic stimuli. J. Comp. Neurol. 2003;467(4):455–463.

54. Brandt MD, Jessberger S, Steiner B, et al. Transient calretinin expression defines early postmitotic step of neuronal differentiation in adult hippocampal neurogenesis of mice. Mol Cell Neurosci 2003;24(3):603–613.

55. Giachino C, Barz M, Tchorz JS, et al. GABA suppresses neurogenesis in the adult hippocampus through GABAB receptors. Development 2014;141(1):83–90.

56. Almeida-Suhett CP, Prager EM, Pidoplichko V, et al. GABAergic interneuronal loss and reduced inhibitory synaptic transmission in the hippocampal CA1 region after mild traumatic brain injury. Exp. Neurol. 2015;273:11–23.

57. Anacker C, Hen R. Adult hippocampal neurogenesis and cognitive flexibility - linking memory and mood. Nat. Rev. Neurosci. 2017;18(6):335–346.

58. Ge S, Pradhan DA, Ming G-L, Song H. GABA sets the tempo for activity-dependent adult neurogenesis. Trends Neurosci. 2007;30(1):1–8.

59. Woodcock T, Morganti-Kossmann MC. The role of markers of inflammation in traumatic brain injury. Front Neurol 2013;4:18.

60. Steenerson K, Starling AJ. Pathophysiology of Sports-Related Concussion. Neurol Clin 2017;35(3):403–408.

61. Garrido-Mesa N, Zarzuelo A, Gálvez J. Minocycline: far beyond an antibiotic. Br J Pharmacol 2013;169(2):337–352.

62. Miao H, Li R, Han C, et al. Minocycline promotes posthemorrhagic neurogenesis via M2 microglia polarization via upregulation of the TrkB/BDNF pathway in rats. J Neurophysiol 2018;120(3):1307–1317.

63. Willis EF, MacDonald KPA, Nguyen QH, et al. Repopulating Microglia Promote Brain Repair in an IL-6-Dependent Manner. Cell 2020;180(5):833-846.e16.

64. Chen X, Duan X-S, Xu L-J, et al. Interleukin-10 mediates the neuroprotection of hyperbaric oxygen therapy against traumatic brain injury in mice. Neuroscience 2014;266:235–243.

65. Fu R, Shen Q, Xu P, et al. Phagocytosis of microglia in the central nervous system diseases. Mol Neurobiol 2014;49(3):1422–1434.

66. Neumann J, Sauerzweig S, Rönicke R, et al. Microglia Cells Protect Neurons by Direct Engulfment of Invading Neutrophil Granulocytes: A New Mechanism of CNS Immune Privilege. J Neurosci 2008;28(23):5965–5975.

67. Shulga A, Magalhães AC, Autio H, et al. The loop diuretic bumetanide blocks posttraumatic p75NTR upregulation and rescues injured neurons. J. Neurosci. 2012;32(5):1757–1770.

68. Parkhurst CN, Yang G, Ninan I, et al. Microglia promote learning-dependent synapse formation through brain-derived neurotrophic factor. Cell 2013;155(7):1596–1609.

69. Rivera C, Voipio J, Thomas-Crusells J, et al. Mechanism of activity-dependent downregulation of the neuron-specific K-Cl cotransporter KCC2. J Neurosci 2004;24(19):4683–4691.

70. Shulga A, Thomas-Crusells J, Sigl T, et al. Posttraumatic GABA(A)-mediated [Ca2+]i increase is essential for the induction of brain-derived neurotrophic factor-dependent survival of mature central neurons. J. Neurosci. 2008;28(27):6996–7005.

71. Caplan HW, Cardenas F, Gudenkauf F, et al. Spatiotemporal Distribution of Microglia After Traumatic Brain Injury in Male Mice. ASN Neuro 2020;12:1759091420911770.

72. Siebold L, Krueger AC, Abdala JA, et al. Cosyntropin Attenuates Neuroinflammation in a Mouse Model of Traumatic Brain Injury. Front Mol Neurosci 2020;13:109.

73. Witcher KG, Bray CE, Chunchai T, et al. Traumatic Brain Injury Causes Chronic Cortical Inflammation and Neuronal Dysfunction Mediated by Microglia. J Neurosci 2021;41(7):1597–1616.

74. Berry C, Ley EJ, Tillou A, et al. The effect of gender on patients with moderate to severe head injuries. J Trauma 2009;67(5):950–953.

75. Coimbra R, Hoyt DB, Potenza BM, et al. Does sexual dimorphism influence outcome of traumatic brain injury patients? The answer is no! J Trauma 2003;54(4):689–700.

76. Jullienne A, Salehi A, Affeldt B, et al. Male and Female Mice Exhibit Divergent Responses of the Cortical Vasculature to Traumatic Brain Injury. J Neurotrauma 2018;35(14):1646–1658.

77. Mollayeva T, Mollayeva S, Pacheco N, Colantonio A. Systematic Review of Sex and Gender Effects in Traumatic Brain Injury: Equity in Clinical and Functional Outcomes. Front Neurol 2021;12:678971.

Figure Legends

Figure 1 Effect of bumetanide on CCI-induced behavioral changes. (A) Schematic representation of the experimental timeline. **(B)** The Object Displacement Task after a 5 min retention time. **(C)** The Novel Object Recognition task after a 1-hour retention time. **(D)** The Novel Object Recognition task after a 5-min retention time. For all experiments, the results are presented as a ratio of time of new versus familiar. n = 10, 11 and 10 respectively. **(E)** Time spent finding the target box in the Barnes Maze. **(F)** Number of entries in different zones of the elevated plus maze. **(G)** Time spent in different zones of the elevated plus maze. n = 3, 5 and 5 respectively. **(H)** Normalized spectral density of delta band in mice 1-month post-CCI. **(I)** Normalized spectral density of theta band. **(J)** Normalized spectral density of gamma band. n=6, 9 and 9 respectively. **(K)** Spike rate of narrow-spiking (NS) units. **(L)** Spiking rate of wide-spiking (WS) units. **(M)** Total number of isolated cells. Data from B were analyzed using the Kruskal-Wallis test. Data from C to G and L to M were analyzed using One-way ANOVA with Dunnett's post hoc test. Data from H to J were analyzed using One-way ANOVA with a Tukey post hoc test *$p < 0.05$; **$p < 0.01$; ***$p < 0.001$.

Figure 2 Effect of bumetanide and minocycline on CCI-induced changes in adult neurogenesis and PV interneuronal loss in the DG. (A) Parvalbumin (PV) labeling (white arrows) at 3 dpCCI in the contralesional (upper pictures) and ipsilesional (lower pictures) DG of sham, CCI vehicle and CCI bumetanide-treated animals (scale bar = 100 µm). **(B)** Quantification of PV-positive cells 3 dpCCI in the contralesional and ipsilesional DG of sham, CCI vehicle and CCI bumetanide-treated animals. **(C)** Same as **(A)** at 7 dpCCI with minocycline-treated animals added. **(D)** Same as **(B)** at 7 dpCCI. **(E)** Doublecortin (DCX, upper pictures) and Nestin (lower pictures) labeling at 7 dpCCI in the ipsilesional DG of sham, CCI vehicle, bumetanide-treated and minocycline-treated animals (scale bar = 100 µm). **(F)** Quantification of DCX-positive cells 7 dpCCI in the ipsilesional DG of sham, CCI vehicle, bumetanide-treated and minocycline-treated animals. **(G)** Quantification of Nestin-positive cells 7 dpCCI in the ipsilesional DG of sham, CCI vehicle, bumetanide-treated and minocycline-treated animals. **(H)** Same as in **(E)** in the contralesional DG. **(I)** Same as in **(F)** in the contralesional DG. **(J)** Same as in **(G)** in the contralesional DG. n = 7 animals per condition, 3 slices per animal. Sets of data from B, D, F, G

and I were analyzed using a one-way ANOVA test with Dunnett's post hoc test. Data from J were analyzed using a Kruskal-Wallis test *p < 0.05; **p < 0.01; ***p < 0.001.

Figure 3 Effect of impaired chloride uptake in microglia morphology and phagocytosis capacity. (A) Average size of primary microglia cells from CX3CR1-Cre ERT2 mice under different conditions: co-transfected with pSico-sh Nkcc1 and pCAG-RFP, treated with bumetanide and tamoxifen, transfected with pCAG-RFP and treated with tamoxifen, co-transfected with pSico-sh Nkcc1 and pCAG-RFP and treated with tamoxifen. n = 4 wells per conditions. 5 cells chosen randomly per well. **(B)** Number of latex beads engulfed by cells in the different conditions. n = 4 wells per conditions. 12 cells chosen randomly per wells. **(C)** Immunostainings of the primary microglia cell culture from CX3CR1-Cre ERT2 mice in the different conditions. Anti-Iba1 was used to label microglial cells (purple), anti-RFP to label the pCAG-RFP plasmid (red), GFP to enhance the pSico-sh Nkcc1 fluorescence (green). YFP was expressed when cells were treated with tamoxifen (green) and the beads were labelled with a Rabbit IgG-DyLight 633 Complex (blue). All data set were analyzed using a one-way ANOVA test with Dunnett's post hoc test. *p < 0.05; **p < 0.01; ***p < 0.001.

Figure 4 Effect of bumetanide on microglia phenotypes and morphological changes after CCI in the DG 3 dpCCI. (A) Total area of Iba1+ cells soma, quantifications of Iba1+ process endpoints, attachment points and length in the ipsilesional DG. n = 5 animals, 2 slices per animal. **(B)** Iba1 immunostaining from sham, CCI-vehicle and CCI-bumetanide treated animals. **(C)** Quantification of the number of contacts between microglia (Iba1 staining) and PV interneurons at 3 dpCCI. n = 5 animals per condition, 3 slices per animal. **(D)** Example of PV and Iba1 immunostaining from sham, CCI-vehicle and CCI-bumetanide treated animals in the ipsilesional DG, 3D representations (upper pictures), and stack (lower pictures). **(E)** Flow cytometry gating plots at 3 dpCCI on the ipsilesional side. **(F)** Analysis of microglia phenotypes by detection of $MHCII^+$ (pro-inflammatory) and $CD206^+$ (pro-phagocytosis) markers by flow cytometry on the ipsilesional side at 3 dpCCI. n = 5-6 animals per condition. **(G)** Quantity of IL-4, IL-10 and IL-6 produced in the ipsilesional hippocampus. Phenotype changes were analyzed by t-test. Number of contacts and morphological analysis (quantified using the ImageJ plugins Neurphology and SynapCountJ) were analyzed using

a one-way ANOVA with Dunnett's post hoc test. Interleukin production was analyzed using a Brown-Forsythe ANOVA with Dunnett's post hoc test *p < 0.05; **p < 0.01; ***p < 0.001.

Figure 5 Effect of bumetanide on microglia phenotypes and morphological changes after CCI in the DG at 7 dpCCI. (A) Total area of Iba1+ cells soma, quantifications of Iba1+ process endpoints, attachment points and length in the contralesional DG 7 dpCCI. n = 5 animals, 2 slices per animal. **(B)** Iba1 immunostaining from sham, CCI-vehicle and CCI-bumetanide treated animals in the contralesional DG. **(C)** Quantification of the number of contacts between microglia (Iba1 staining) and PV interneurons at 7 dpCCI. n = 5 animals per condition, 3 slices per animal. **(D)** Example of PV and Iba1 immunostaining, from sham, CCI-vehicle and CCI-bumetanide treated animals in the contralesional DG, 3D representations (upper pictures), and stack (lower pictures). **(E)** Analysis of microglia phenotypes by detection of $MHCII^+$ (pro-inflammatory) and $CD206^+$ (pro-phagocytosis) markers by flow cytometry on the contralesional side at 7 dpCCI. n = 5-6 animals per condition. **(F)** Quantity of IL-4, IL-10 and IL-6 produced in the contralesional hippocampus. **(G)** Quantification of Bdnf signal intensity within microglia of the ipsi- and contralesional brain of Sham Veh, Sham Bum, CCI Veh and CCI Bum treated animals. **(H)** Example of Iba1 and Bdnf staining in DG of Sham and CCI animals treated with bumetanide or vehicle. **(I)** Example of Iba1 and Bdnf staining in a single microglial cell. N = 3, 3 slices per animal. Phenotype changes were analyzed by Student's t-test. Number of contacts and morphological analysis (quantified using the ImageJ plugins Neurphology and SynapCountJ) were analyzed using a one-way ANOVA with Dunnett's post hoc test. Interleukin production was analyzed using a Kruskall-Wallis test for IL-10. *p < 0.05; **p < 0.01; ***p < 0.001.

Figure 6 Effect of bumetanide on post-injury microglia surveillance monitored by 2-photon *in vivo* imaging. (A) Schematic representation of the experimental timeline. **(B)** Maximal projection of image at 1 and 5 days after laser induced focal injury. Lower panel showing a single microglia cell and the corresponding temporal color-coded projection (recorded time of 1 h at 5 min intervals). **(C)** Quantification of process length at 1 and 5 days after laser induced focal injury in the presence and absence of bumetanide. **(D)** Same as **(B)** in bumetanide-treated animals in bumetanide-treated animals. Lower panel showing one single microglia and the corresponding

temporal color-coded projection (recorded time of 1 h at 5 min intervals). (E) Quantification of motility ratio at 1 and 5 days in the presence and absences of bumetanide. All data was analyzed using unpaired Student's t-test. *p < 0.05.

Figure 7 Effect of pre-CCI bumetanide treatment on PV interneuron survival. (A) Quantification of parvalbumin (PV) positive cells 1 dpCCI in the contralesional and ipsilesional DG of sham, CCI vehicle and CCI bumetanide animals treated for 7 days before CCI. n = 3, 5 and 5 respectively, 3 slices per animal. **(B)** PV labeling at 1 dpCCI in the contralesional and ipsilesional DG of sham, CCI vehicle and CCI bumetanide animals, treated for 7 days before CCI (scale bar = 100 µm). All data set were analyzed using a one-way ANOVA with Dunnett's post hoc test. *p < 0.05; **p < 0.01; ***p < 0.001.

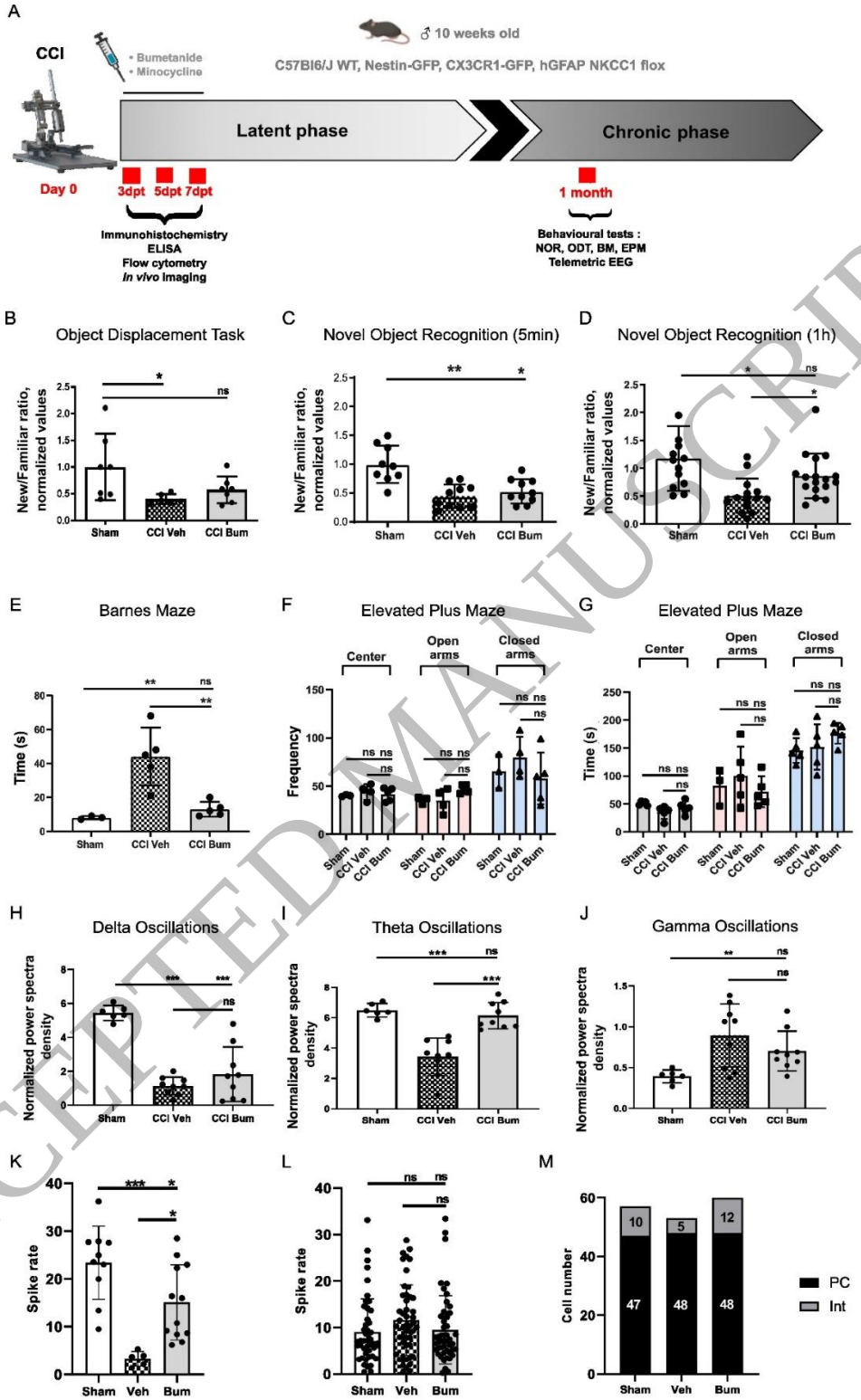

Figure 1
147x247 mm (x DPI)

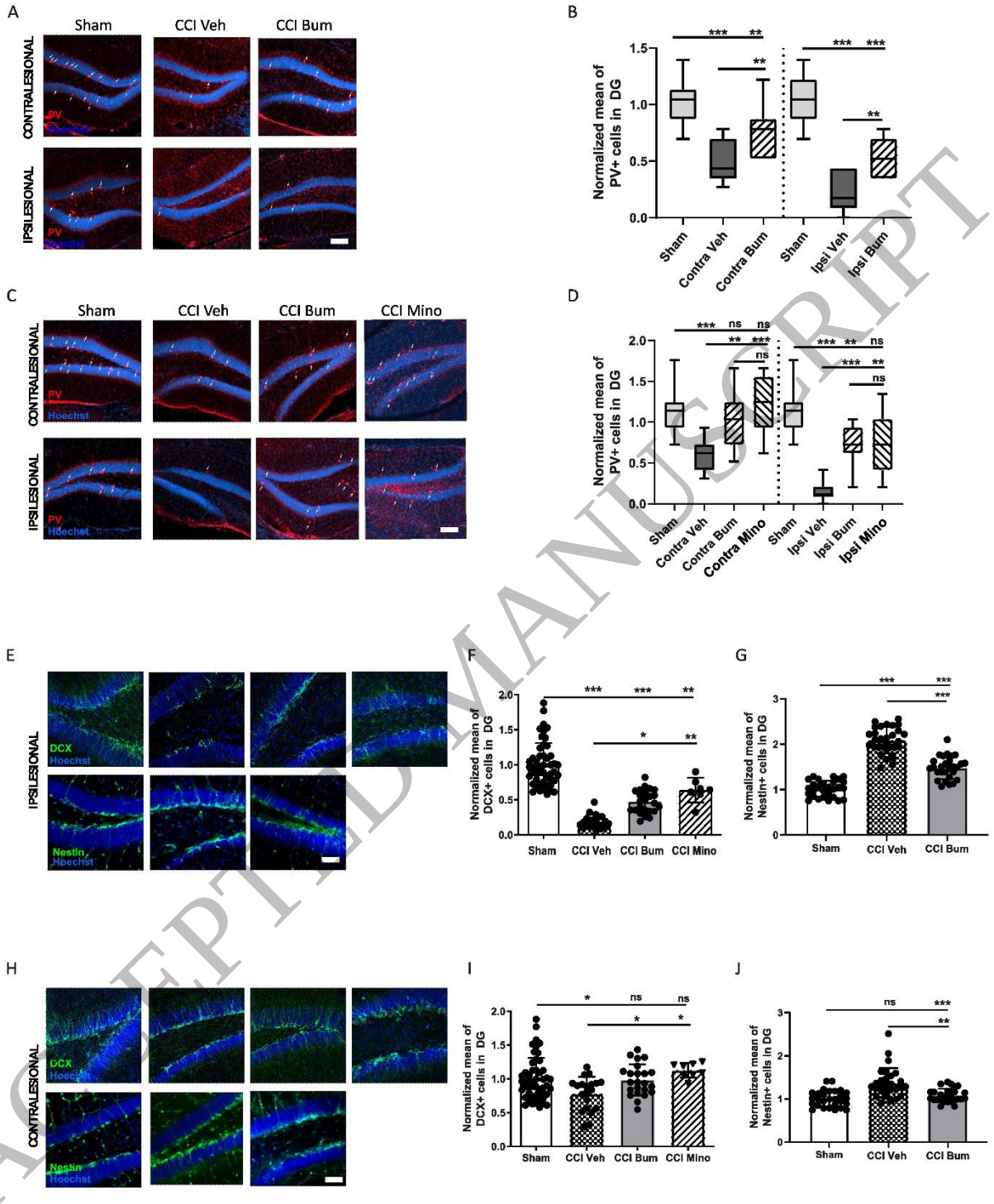

Figure 2
160x198 mm (x DPI)

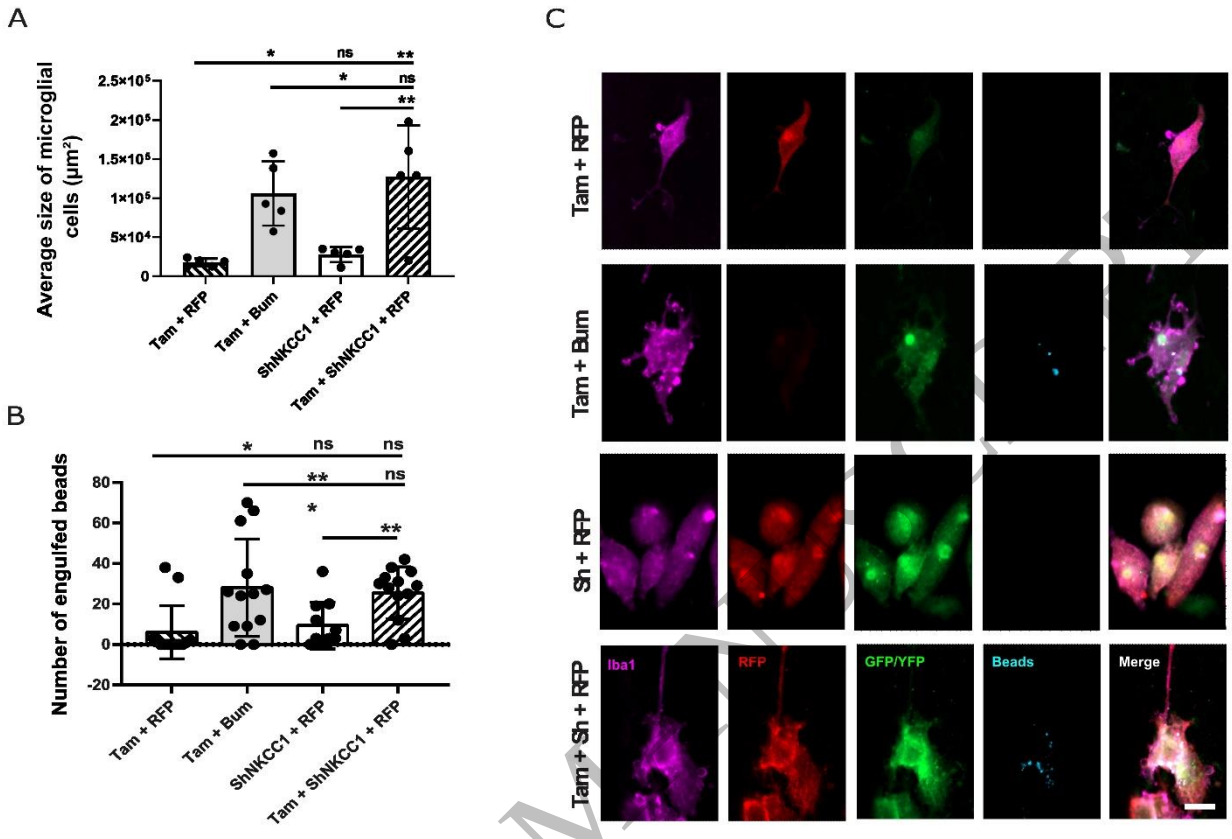

Figure 3
145x247 mm (x DPI)

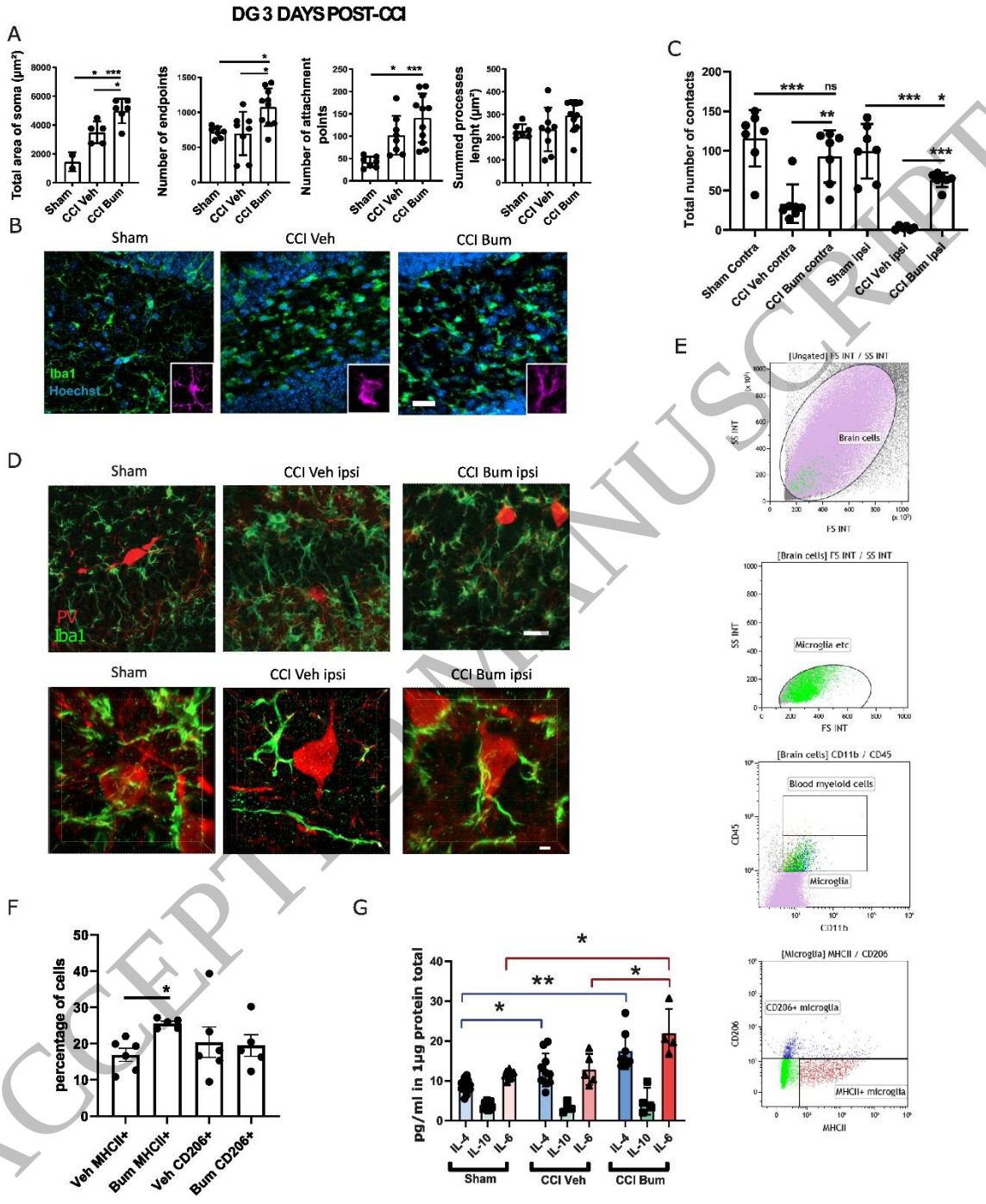

Figure 4
160x198 mm (x DPI)

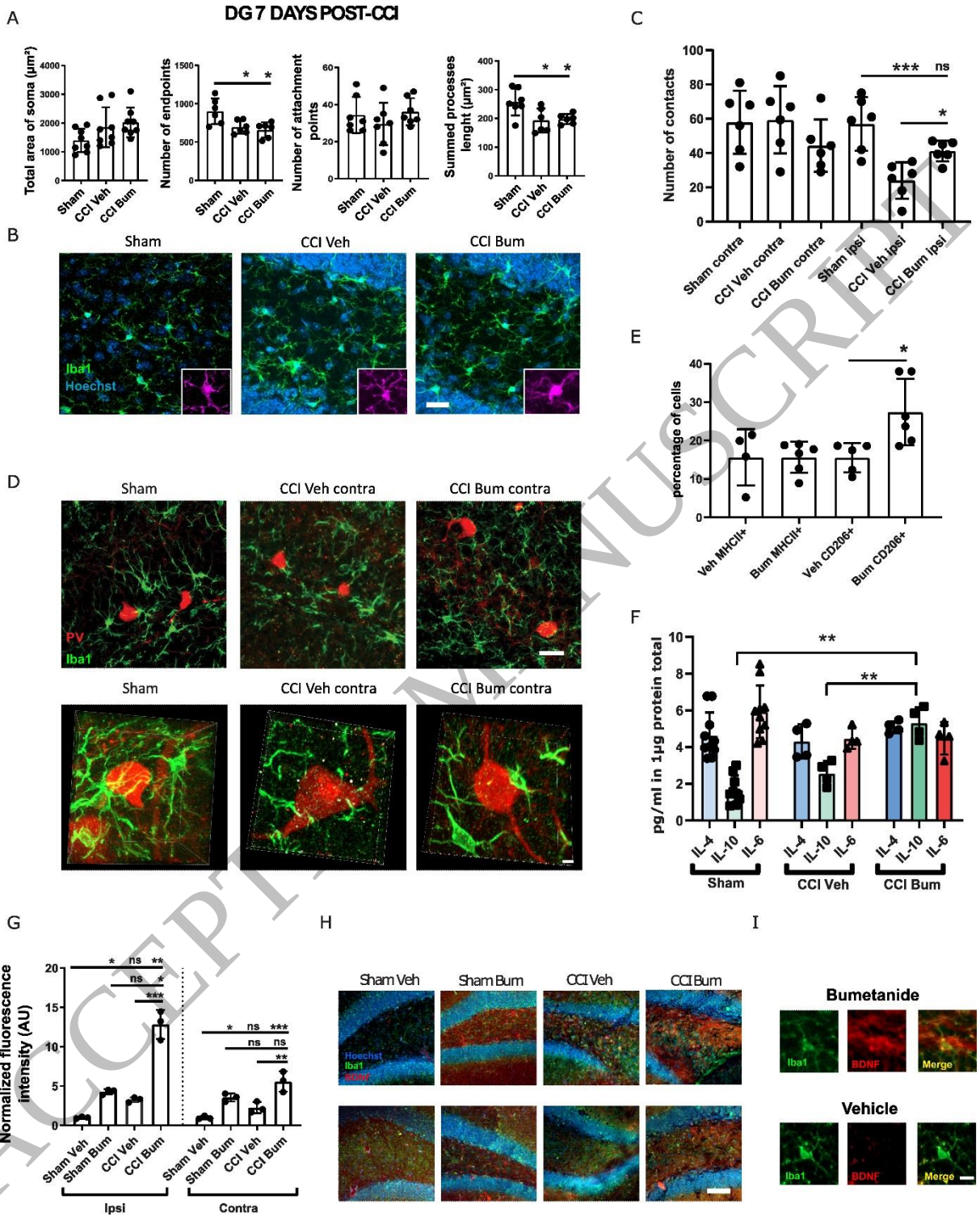

Figure 5
160x198 mm (x DPI)

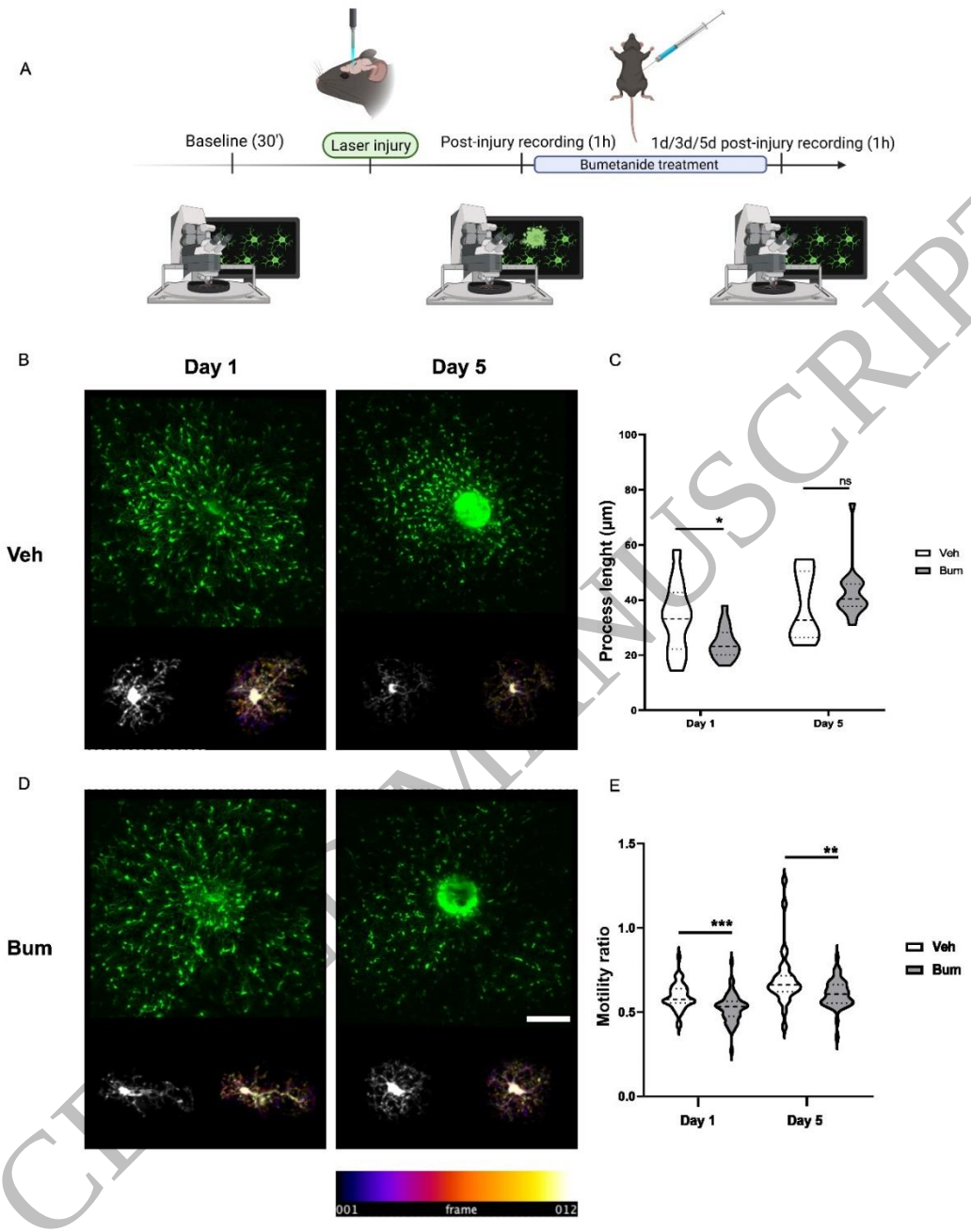

Figure 6
160x226 mm (x DPI)

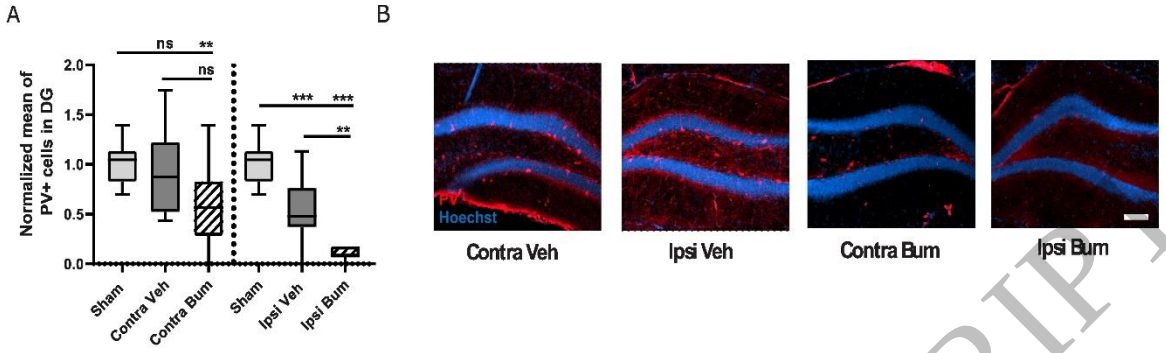

1

2 *Figure 7*
3 *160x226 mm (x DPI)*